ACS Catalysis

pubs.acs.org/acscatalysis Research Article

A Thiadiazole-Based Covalent Organic Framework: A Metal-Free Electrocatalyst toward Oxygen Evolution Reaction

Sujan Mondal,[▽] Bishnupad Mohanty,[▽] Maryam Nurhuda, Sasanka Dalapati, Rajkumar Jana, Matthew Addicoat, Ayan Dutta, Bikash Kumar Jena,* and Asim Bhaumik*

Cite This: https://dx.doi.org/10.1021/acscatal.9b05470 Read Online

ACCESS | Metrics & More | Article Recommendations | Supporting Information

ABSTRACT: Covalent organic frameworks (COFs) have attracted surging interest lately due to their wide potential in several frontline application areas like gas storage, sensing, photovoltaics, fuel cells, active catalyst supports, and so on. However, only very few reports are available for the metal-free electrocatalysis over COFs. Herein, we developed a new thiadiazole-based COF, C4-SHz COF, through the reaction between 1,3,5-tris(4-formylphenyl)benzene and 2,5-dihydrazinyl-1,3,4-thiadiazole that possesses a very high specific surface area of 1224 $m^2\ g^{-1}$, unique molecular architecture, high porosity, and abundant active sites. The as-synthesized C4-SHz COF displayed superior electrocatalytic oxygen evolution reaction (OER) activity and excellent long-term durability. The electrocatalytic performance of the C4-SHz COF achieved a current density of 10 mA/cm^2 at an overpotential of 320 mV. The higher activity of the C4-SHz COF could be attributed to the high Brunauer−Emmett−Teller surface area, porosity, and network structure of the π-conjugated organic building blocks, which allowed fast charge and mass transport processes. This work validates the promising potential of a metal-free COF electrocatalyst toward the OER and its capability to replace carbon-based electrocatalysts.

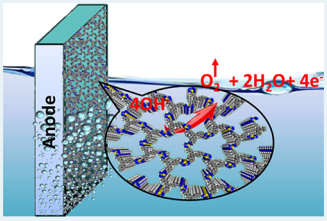

KEYWORDS: *covalent organic frameworks (COFs), thiadiazole moiety, metal-free electrocatalyst, oxygen evolution reaction (OER), water splitting*

■ INTRODUCTION

Rapid decay of fossil fuels combined with environmental crises associated with carbon emissions significantly affected the economy and ecology of the whole world. Thus, the demand for renewable energy is surging over the years, and electrochemical water splitting can be considered as a green and promising technology[1] to overcome this problem. The electrochemical water splitting plays a crucial role in advanced energy technologies, such as solar fuel production, supercapacitor, metal−air batteries, etc.[2−5] Still, water oxidation (oxygen evolution reaction, OER) requires a higher energy input due to the involvement of the multi-electron transfer reaction pathway and its low efficiency. Hence, the commercialization of water splitting technology requires stable, highly active, and low-cost water oxidation electrocatalysts. Currently, precious transition metal oxide-based electrocatalysts such as RuO_2 and IrO_2 are highly active toward the OER from alkaline water. However, high cost, scarcity, and low stability hamper the utilization of clean and sustainable energy technologies[6,7] in this context. Thus, for the past couple of years, extensive efforts have been devoted for the development of earth-abundant, low-cost, and efficient transition metal-based electrocatalysts such as oxides, chalcogenides, phosphides, nitride, metal-free catalysts, etc., for the OER.[8−14] However, most of the transition metal-based catalysts still suffer from lower catalytic activity, inferior conductivity, and poor operational durability.

Simultaneously, over the past few years, intensive research has been carried out for developing efficient metal-free catalysts.[2,3] Metal-free electrocatalysts have several unique advantages, such as their environment-friendly nature, earth-abundant, cost-effective, and resistance to a wide pH range. For electrochemical OER applications, several metal-free catalysts have been developed in recent times.[15−17] Among different metal-free porous nanomaterials, covalent organic frameworks (COFs)[18,19] are the emerging class of porous organic polymers with precisely controllable structural motifs linked through covalent bonds. COFs possess extraordinary properties like large surface area, high crystallinity, tunable pore size, and unique molecular architecture.[20−24] Due to these unique properties, COFs have been used in a wide range of applications.[25−27] High surface area, tunable structures with appropriate building blocks, and porous nature of the COFs made them ideal for electrocatalysis.[28] Accordingly, substantial progress has been made for the design and synthesis of COFs from low-cost monomer precursors. Till now, COFs have been explored as a support material of graphene, conductive carbon,

Received: December 18, 2019
Revised: March 23, 2020

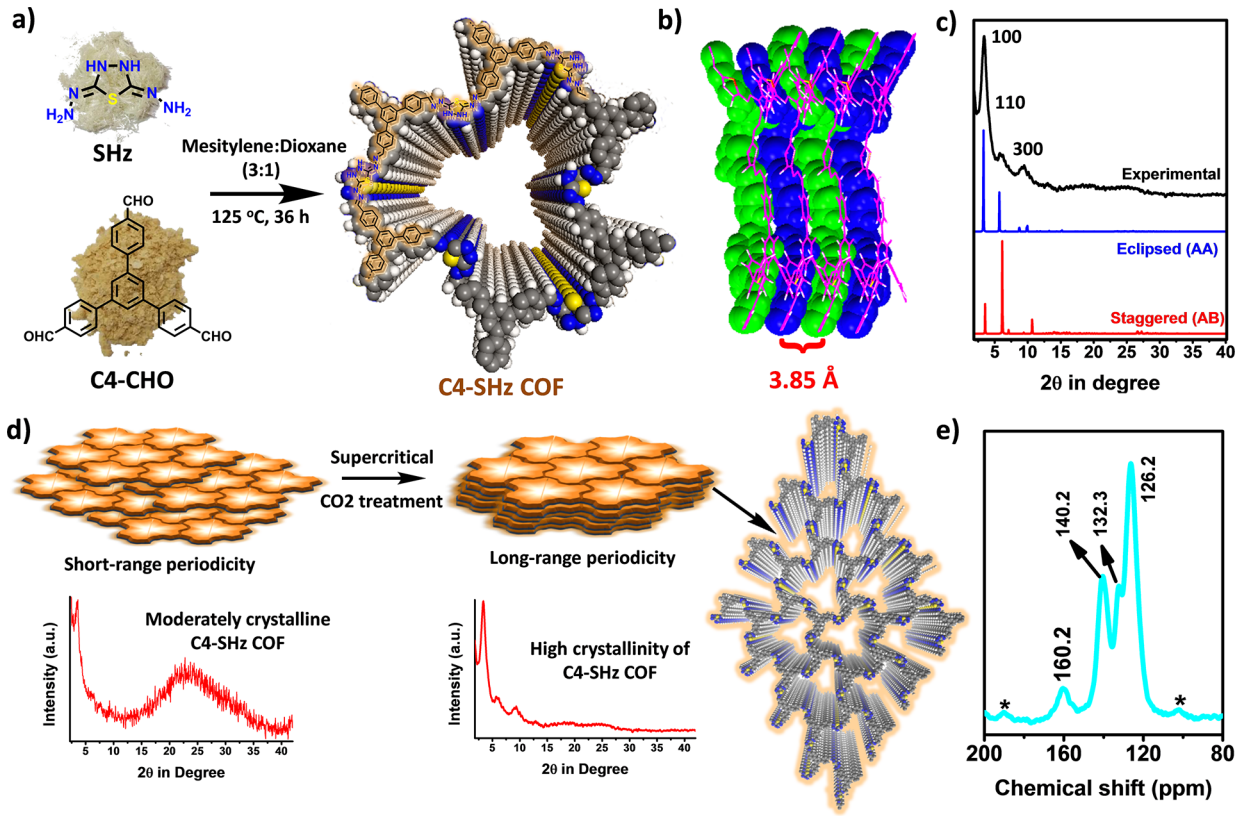

Figure 1. Schematic presentation of the COF (a) proposed structure and (b) packing diagram. (c) Comparison of experimental PXRD pattern of the crystalline C4-SHz COF with simulated PXRD patterns of the C4-SHz COF. (d) Graphical representation of switching shortly to long-range periodicity. (e) Solid-state ^{13}C MAS NMR spectrum of the COF; the spinning sidebands are represented by asterisks.

carbon nanotubes (CNTs), etc., for electrocatalytic applications. For example, Kamiya et al. have reported covalent triazine frameworks as support materials for Pt nanoparticle and studied its ORR activity.[29] Mullangi et al. used flexible COFs as support materials for electrocatalytic OER applications.[28] Similarly, Aiyappa et al. designed Co-COF and studied its OER activity,[30] whereas Fe and Co NPs supported over COFs have been employed in electrochemical oxygen reduction reaction (ORR).[31] Although there are very few reports on the usage of COFs as photocathodes for light-induced hydrogen evolution reaction (HER) via water splitting,[32] the use of a crystalline COF as a metal-free OER electrocatalyst has been rarely explored till date.[33]

In this article, we have introduced an unprecedented imine-linked thiadiazole-based crystalline COF (C4-SHz COF) and explored its catalytic activity in the electrochemical water oxidation reaction. Through the general solvothermal protocol (Schiff base condensation using acetic acid),[26,27,30] a nitrogen-rich thiadiazole moiety has been incorporated in the polymeric backbone of the C4-SHz COF, which exhibited superior activity toward OER. The relevant characterization data suggested that the C4-SHz COF possesses a high specific surface area and crystalline metal-free organic framework structure. The newly developed COF displayed an excellent electrocatalytic activity and durability under alkaline pH conditions, which is comparable to the other metal-free electrocatalysts reported so far.

RESULTS AND DISCUSSION

The thiadiazole-based imine-linked COF (C4-SHz COF) was synthesized through the general Schiff base condensation polymerization between 1,3,5-tris(4-formylphenyl)benzene (C4-CHO) and 2,5-dihydrazinyl-1,3,4-thiadiazole (SHz) under the solvothermal condition for 36 h (Figure 1a and Figures S1−S3, Supporting Information). The resultant as-synthesized imine-linked framework has shown a low sign of crystallinity (Figure 1d), and this could often occur due to the self-assembly through weak $\pi-\pi$ stacking interaction of individual COF layers. To get the well-defined molecular stacked framework, the as-synthesized C4-SHz COF material was activated using supercritical carbon dioxide treatment following the reported protocol by Medina et al.[34] The more prominent desired peaks in X-ray diffraction for the post-activated material is observed (Figure 1d), suggesting the well-defined structure of pores. Surprisingly, the measured S_{BET} values are also mirroring this trend by narrowing the pore size (Figure S4, Supporting Information).

The crystalline structure of the C4-SHz COF is resolved through the experimental powder X-ray diffraction measurement in combination with theoretical simulations and Pawley refinement (Figure S5 and Tables S1 and S2, Supporting Information). As seen in Figure 1c, a distinct peak at $2\theta = 3.3°$ is assigned to the 100 crystal plane of the COF. Additionally, relatively weak peaks at $2\theta = 5.8$ and 9.9° correspond to the reflection from 110, and 300 planes are also observed. The weak broad peak centered at $2\theta = 20-26°$ (002 plane) is possibly due to the interlayer $\pi-\pi$ stacking of the COF, and distances between the individual 002 planes are ca. 3.85 Å

https://dx.doi.org/10.1021/acscatal.9b05470
ACS Catal. XXXX, XXX, XXX−XXX

(Figure 1b). A probable 2D model structure was constructed using Materials Studio 7 in the *P*1 space group. An asymmetric unit in the crystal structure and graphical representation of the 2D layered COF is shown in Figure S6 (Supporting Information). The simulated PXRD pattern of the eclipsed AA stacking model is well fitted with the experimental diffraction data (Figure 1c). In contrast, the PXRD pattern obtained from the AB stacking model deviates from the experimentally observed data, especially in terms of peak intensity ratios. The perfect agreement in favor of the experimental X-ray pattern was further confirmed by Pawley refinement [R_{wp} = 7.23%, Rp = 5.32%] (Figure S5). The unit cell parameters were as follows: a = 31.00 Å, b = 31.46 Å, c = 7.70 Å; α = 99.26°, β = 87.67°, and γ = 120.51°.

The specific surface area and porous nature of the C4-SHz COF were examined by conducting N_2 adsorption−desorption analysis at 77 K. As shown in Figure 2a, the C4-SHz COF

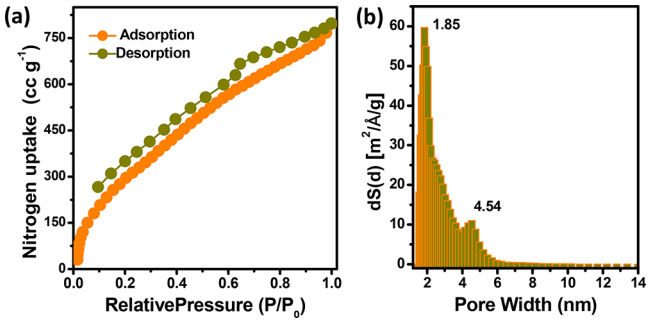

Figure 2. (a) N_2 adsorption−desorption analysis of the C4-SHz COF and (b) NLDFT pore size distribution plots.

exhibits a combination of type I and IV isotherms. A significant nitrogen uptake at low relative pressures (P/P_0 < 0.03) followed by a gradual increase in adsorption at a higher P/P_0 value suggested the distinctive features for the coexistence of micropores and mesopores along with interparticle pores.[35−38] The corresponding pore size distribution plot (Figure 2b), as determined from the adsorption branch of the isotherm based on nonlocal density functional theory (NLDFT), revealed the presence of micropores and mesopores in our C4-SHz COF material. The calculated BET (Brunauer−Emmett−Teller, S_{BET}) surface area from this isotherm was 1224 m^2 g^{-1}, and the total pore volume was 1.12 cc g^{-1}. The simulated BET surface area of the AA stacked model of the C4-SHz COF has been computed using the DFTB calculations. The corresponding simulated specific surface area was found to be 2339 m^2 g^{-1} (Figure S7, Supporting Information). The noticeable distinction in BET surface area from the experimental data is related to the crystallinity of the COF material, and such deviations were also reported for other imine-based COFs.[39−42]

The structural growth and imine linkage formation of the COF are confirmed by FTIR and ^{13}C MAS NMR analyses. In the FTIR spectrum of the C4-SHz COF (Figure 3a), the absorption band at 1693 cm^{-1} corresponded to C═N absorption, which is also confirmed by the resonance signal at 160.2 ppm in ^{13}C NMR. The peak at 3416 cm^{-1} could be attributed to N−H stretching vibration. The complete utilization of the aldehyde sources was confirmed by the missing peak at 1698 cm^{-1} in the IR spectrum and the absence of aldehydic resonance peak at 190 ppm in ^{13}C NMR. In the

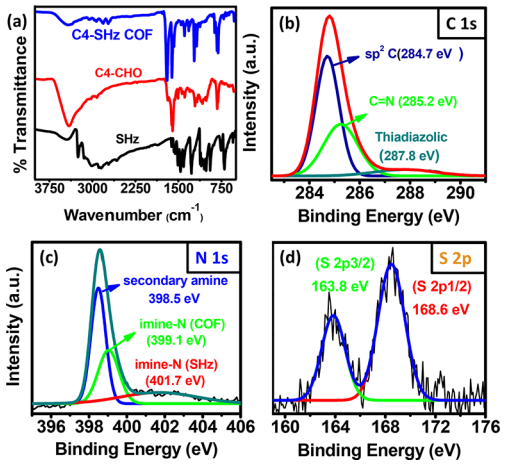

Figure 3. (a) IR spectrum of the C4-SHz COF along with the spectra of SHz and C4-CHO. (b) C 1s X-ray photoelectron spectroscopy (XPS). Deconvoluted high-resolution (c) N 1s XPS spectra and (d) S 2p XPS spectra of the thiadiazole-based COF.

spectrum in Figure 1e, the resonance signal at 160.2 ppm is ascribed to the carbon atom adjacent to the S atom of the SHz moiety. The peak at 140.2 ppm is indicative of substituted quaternary carbons of the polymeric network. The resonance peak at 132.3 ppm is attributed to the carbon atom of the aldehyde moiety that connected to the imine carbon of the organic framework. The additional peak at 126.2 ppm appeared due to the sp^2-hybridized aromatic carbons.

To gain further information about the surface chemistry and chemical composition, we have carried out the XPS analysis of the C4-SHz COF. As shown in Figure 3c, the N 1s spectrum can be deconvoluted into three component peaks ascribed to secondary amine (−NH) of the SHz moiety (398.5 eV), imine−N (399.1 eV) of the newly formed COF networks, and imine−N (401.7 eV) of the SHz moiety.[41] The C nuclei with different environments were investigated by a deconvoluted high-resolution C 1s XPS scan (Figure 3b). The major component at 284.7 eV is attributed to the aromatic sp^2 C atom. Another component at 285.2 eV can be assigned to the N atom associated with imine linkage. The peak at a higher binding energy (287.8 eV) is probably due to thiadiazolic C of the COF. Strong characteristic S 2p doublet peaks (Figure 3d) were observed at 163.8 (S 2p3/2) and 168.6 eV (S 2p1/2).[43]

The thermal stability of the covalent framework was estimated by using thermogravimetric analysis (TGA) under the aerobic environment. As seen from Figure S8 (Supporting Information), an initial weight loss could be assigned to the trapped guest molecule in the porous framework. Then, with the continuous increase in temperature, the organic framework is stable up to 350 °C. With a further increase in temperature, a continuous weight loss is associated with the burning of organics present in the material. The representative FESEM (Figure 4a) and HRTEM (Figure 4b) images of the as-synthesized thiadiazole COF have clearly shown regularly their spherical morphology with diameters of 0.5−0.8 μm. After the supercritical CO_2 activation, it was observed that the smooth spherical surface of the as-synthesized COF material transformed to the microflower-shaped structure (Figure 4c−f) with the size distribution of 1.2−1.8 μm. This is also reflected by the nitrogen sorption isotherm with enhancing the BET surface area (Figure S4).

https://dx.doi.org/10.1021/acscatal.9b05470
ACS Catal. XXXX, XXX, XXX−XXX

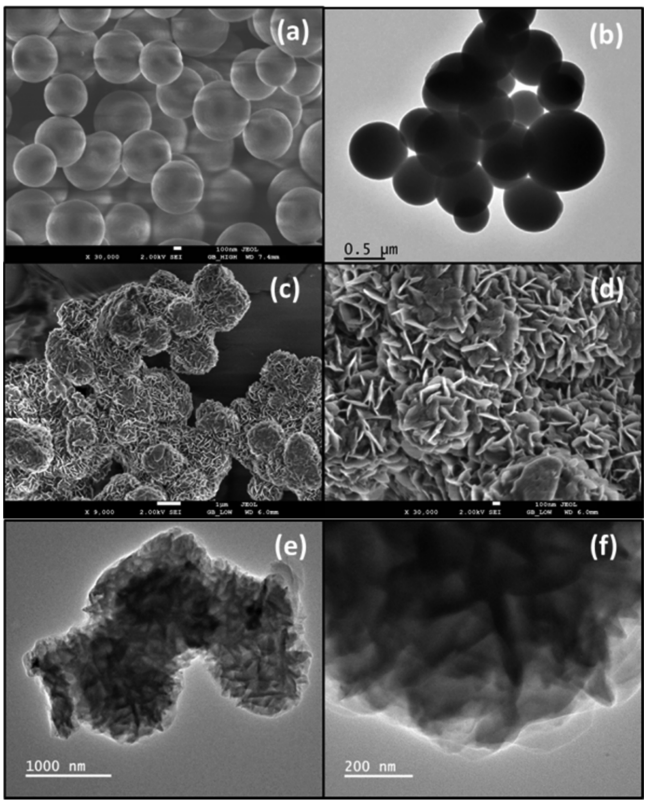

Figure 4. FESEM micrographs of the (a) as-synthesized and (c, d) crystalline C4-SHz COF. Representative TEM images of the (b) as-synthesized and (e, f) crystalline C4-SHz COF material.

To determine the electrocatalytic OER activity of the as-synthesized catalyst, linear sweep voltammetry (LSV) was recorded. The OER activity of the C4-SHz COF was compared with the state-of-the-art catalyst IrO_2/C and bare GCE under similar conditions. Before the LSV measurement, the C4-SHz COF catalyst was electrochemically preconditioned to reach a stable state (Figure S9, Supporting Information). All the LSV plots are presented after *iR* compensation. The *iR* compensation process is explained in the Supporting Information (Figure S10). Figure 5a presents the *iR*-compensated LSV polarization plots. As expected, the bare glassy carbon electrode (GCE) exhibits a very low anodic current density with higher overpotential values, suggesting its negligible OER activity. The C4-SHz COF-modified GCE shows a sharp increase in the anodic current density, which indicates its intrinsic OER activity. For electrocatalytic activity, the overpotential (η) gives an idea about the extent of polarization upon passage of the faradic current and reflects the efficiency of the catalysts. The catalyst C4-SHz COF possesses the higher activity with a lower onset overpotential of 250 mV, which is higher than that of benchmark catalyst IrO_2/C. The current density of 10 mA/cm^2 is the critical value for driving solar fuel conversion and used as a benchmark for comparing electrocatalytic performance. The as-synthesized C4-SHz COF achieved a current density of 10 mA/cm^2 at a lower overpotential of 320 mV, which is lower than benchmark catalyst IrO_2/C. The overpotential of the C4-SHz COF is comparable with most of the reported metal-free OER electrocatalysis (Table S3, Supporting Information). This result suggests the promising electrocatalytic activity of the highly crystalline C4-SHz COF toward the OER. The OER activity is also compared with a moderately crystalline C4-SHz COF. The highly crystalline C4-SHz COF exhibits a lower overpotential with enhanced current density in comparison to moderately crystalline C4-SHz COF (Figure S11, Supporting Information). Further, the OER activity of the highly crystalline C4-SHz COF is checked in different conditions, i.e., acidic (0.5 M H_2SO_4) and neutral (1 M PBS) solutions. The C4-SHz COF exhibits the higher OER activity in 1 M KOH (Figure S12, Supporting Information).

The reaction dynamics and mechanism of the as-synthesized catalysts toward the OER were investigated by measuring the

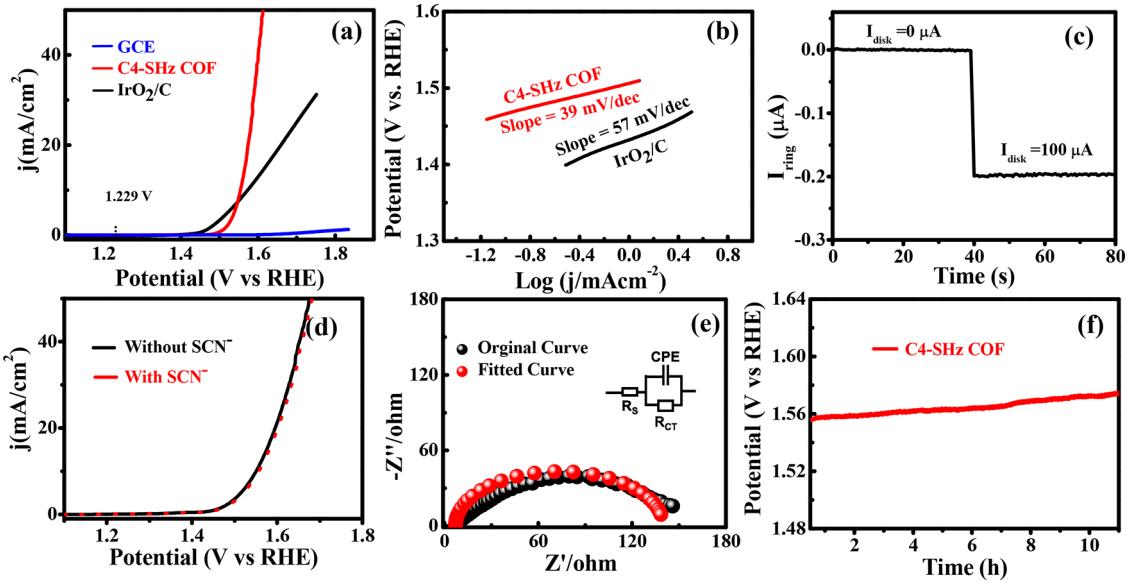

Figure 5. OER performance of the catalysts in 1 M KOH with a scan rate of 5 mV/s. (a) LSV polarization plots of the C4-SHz COF, IrO_2/C, and GCE. (b) Tafel plots of the C4-SHz COF and IrO_2/C. (c) Faradic efficiency calculation of the C4-SHz COF by using the RRDE technique. (d) LSV polarization plot of the C4-SHz COF before and after the addition of 10 mM KSCN. (e) EIS Nyquist plot for the C4-SHz COF. (f) Chronopotentiometry measurement shows the stability of C4-SHz COF.

https://dx.doi.org/10.1021/acscatal.9b05470
ACS Catal. XXXX, XXX, XXX−XXX

Tafel slope from Tafel plots. The Tafel plots are obtained from the LSV measurements and reflect the relationship between the overpotential (η) and the log of current density. The Tafel slope is derived from the linear part of the Tafel plot, and lower the Tafel slope value indicates the higher electrocatalytic activity. The C4-SHz COF exhibits the lower Tafel slope of 39 mV/dec, which is lower than that for IrO_2/C (57 mV/dec) (Figure 5b). The Tafel slope of the C4-SHz COF is lower than that of other reported metal-free catalysts. The exchange current density (j_0) of the C4-SHz COF is calculated from the Tafel plot by the extrapolation method (Figure S13, Supporting Information). The exchange current density (j_0) of the C4-SHz COF is estimated to be 3.95×10^{-4} mA/cm^2. The value of j_0 is also proportional to the electrochemically active surface area. The small Tafel slope and large exchange current density indicate that the C4-SHz COF can produce superior metal-free OER performance. The faradic efficiency (FE) of the catalysts is measured by the rotating ring-disk electrode (RRDE) experiment.[44,45] The RRDE experimental details are discussed in the Supporting Information. The FE is calculated from the ratio of the ring current to the disk current (eq S3, Supporting Information). A constant current of 100 μA is applied to the disk electrode, and a 19.6 μA current was generated at the ring electrode (Figure 5c), which corresponds to the promising FE of the C4-SHz COF (98%). The formation of the oxygen bubble during the OER was supported by the polarization curve of the oxygen reduction reaction (ORR) collected from the ring electrode at a constant disk potential of 1.50 V (Figure S14a, Supporting Information). The number of electron transfer during the OER was also calculated from the RRDE measurement. During OER polarization, a very negligible current density was observed in the ring electrode that is assigned to the electro-oxidation of generated H_2O_2 (Figure S14b). This observation validates the four-electron pathway for the OER.

Generally, the precursor used for the synthesis of the COF or the electrolyte used for testing the electrocatalytic activity contains some metal catalysts (i.e., Fe^{3+}), and it may contribute toward the OER activity of the as-synthesized materials. To rule out the contribution of metal ions (i.e., Fe^{3+}), SCN^- tests were carried out. The LSV data of the C4-SHz COF is collected before and after the addition of the SCN^- ions, and it suggests that SCN^- ions did not affect the OER activity, i.e., the OER activity is due to the metal-free C4-SHz COF catalyst (Figure 5d). This suggests that both the C4-SHz COF and electrolyte (KOH) are free from metal impurities.[14] The enhanced catalytic activity of the C4-SHz COF was further accessed by calculating active sites and the intrinsic catalytic activity. Therefore, we explored the mass activity, specific activity, electrochemically active surface area (ECSA), and roughness factor (R_f) of C4-SHz COF catalysts. At η = 320 mV, the mass activity and specific activity for the C4-SHz COF catalyst were found to be 286 A g^{-1} and 0.011 mA/cm^2, respectively. To measure the electrochemically active surface area (ECSA) and roughness factor, electrical double layer capacitance (Cdl) of the C4-SHz COF was evaluated by measuring the CV in the non-faradic region at scan rates of 10−100 mV/s in 1 M KOH at a potential ranging from 0 to 0.1 V (Ag/AgCl) and is shown in Figure S15a, Supporting Information. The value of Cdl is estimated from the linear slope and found to be 2.75 mF cm^{-2} (Figure S15b, Supporting Information). The ECSA and R_f values of the C4-SHz COF were estimated to be 68.75 cm^2 and 968.30, respectively. Thus, the C4-SHz COF shows a high electrochemical catalytic surface area that may be due to the exposed excess nitrogen atom on the surface, which plays as the active sites for the OER activity. The high surface area and the porous structure can facilitate the diffusion of the electrolyte to access more number of reactant species on the electrode surface that resulted in an enhanced performance during the OER. The high mass and specific activity of the C4-SHz COF may also be associated with fast charge transfer during the OER process. The electrochemical impedance spectroscopic (EIS) Nyquist plot of the C4-SHz COF is also presented in Figure 5e. The smaller polarization resistance of the C4-SHz COF indicates the higher charge transfer kinetics and faster electron transfer process that supports the OER activity.[46] The durability is another key factor to evaluate the catalytic activity in practical application. The long-term durability of the C4-SHz COF has been studied by chronopotentiometry measurements. The time-dependent chronopotentiometry measurements demonstrate that the C4-SHz COF is a stable material and can work efficiently for more than 11 h at a current density of 10 mA/cm^2 (Figure 5f). Further, the stability of the C4-SHz COF at higher current densities (20 and 50 mA/cm^2) has been checked with time-dependent chronopotentiometry measurement (Figure S16, Supporting Information). The as-synthesized material shows a quite stable response at higher current densities as well. The above measurements demonstrate the enhanced efficiency and robustness of the C4-SHz COF toward the OER and validate its promising application in future energy devices. It is quite essential to understand the structure, morphology, and any alternation of the bonding connectivity of the C4-SHz COF after the durability test. The post-OER analysis validates the robust properties of the electrocatalyst for practical application. Therefore, PXRD and FTIR analyses have been carried out after the stability test. In the PXRD patterns, no change in the crystal phase was observed (Figure S17, Supporting Information). This result suggested the stability of the crystalline COF structure in the electrocatalyst. FTIR spectra confirm the retention of the bonding connectivity within the organic framework (Figure S18, Supporting Information) after the OER stability test, suggesting the C4-SHz COF as a robust material.

The mechanism of the OER process and the efficiency of the C4-SHz COF material toward the electrochemical OER are rationalized through a density functional theory study based on first-principle calculations using the VASP simulation package. We have constructed a periodic monolayer model of C4-SHz o (cell size: 31.09 × 27.22 Å^2) consisting of 123 atoms, as shown in Figure 6a. The efficiency of the OER can be determined by calculating the reaction free energies of the individual elementary steps.[47] Therefore, the free-energy change for the adsorption of the intermediates (i.e., OH*, O*, and OOH*) on the C4-SHz surface has been calculated, and free-energy profiles for OER pathways at U = 0 and 1.23 V are given in Figure 6c. For OH^- adsorption on the C4-SHz surface, there are seven possible sites, including the S atom (Figure 6b and Figure S19, Supporting Information). However, adsorption of OH^- is more favorable on the C2 site with the highest OH^- adsorption energy of −1.61 eV (Figure 6b and Table S4). However, there are very weak interactions between OH^- and either the N3 or S site (Figure S19e,f). Therefore, the active site for OH^- adsorption is predominantly the C2 site. From the free-energy profile diagram (Figure 6c), it is evident that OOH* adsorption with the highest (most positive) free-energy

https://dx.doi.org/10.1021/acscatal.9b05470
ACS Catal. XXXX, XXX, XXX−XXX

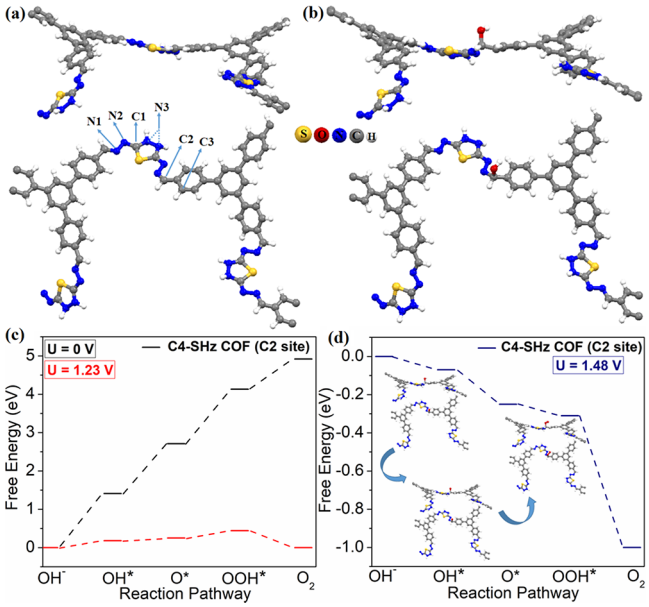

Figure 6. (a) Theoretically optimized structure of the C4-SHz monolayer (different C and N sites are marked) and (b) most stable structure of the OH* adsorbed C4-SHz surface (all other possible OH^- adsorption sites are shown in Figure S19, Supporting Information). (c) Free-energy profile for the OER pathway in alkaline medium on the C2 site at $U = 0$ and 1.23 V for the C4-SHz COF. (d) Free-energy profile at the experimentally determined onset potential, i.e., at an applied bias of $U = 1.48$ V (inset shows the structures of adsorption intermediates OH*, O*, and OOH* on the C2 site of the C4-SHz surface).

value is the rate-determining step during the OER process for the C4-SHz COF.[47]

The free-energy values of OOH* adsorption on the C4-SHz surface are 4.13 and 0.44 eV at $U = 0$ and 1.23 V. This finding is consistent with the earlier reported COF material as the metal-free OER electrocatalyst.[33] To get further insight about the excellent electrocatalytic activity of the C4-SHz COF, we have performed density of states (DOS) analysis. Total and projected density of states (TDOS and PDOS) analysis clearly demonstrates that the VBM is mainly composed of the 2p orbital of C atoms, whereas the 2p orbitals of heteroatoms, i.e., N and S atoms, contribute to the CBM (Figure S20, Supporting Information). Among various C sites, as evident from Figure S20b, the major contribution to the VBM comes from the C2 sites. Therefore, upon adsorption of energy, holes will be generated mainly on C atoms (especially on the C2 atom), and heteroatom sites will be electron-rich. For the OER process in alkaline medium, OH^- is oxidized to O_2 after absorbing holes from the active C2 sites, which is consistent with previously reported COFs and heteroatom-doped graphene systems.[33,48,49] Besides, we have determined the free-energy profile for the OER pathway at an applied bias of 1.48 V (Figure 6d), which is the experimentally determined onset potential. Interestingly, the energy profile diagram exhibits the downhill OER pathway at $U = 1.48$ V, validating the experimental findings of the OER onset overpotential. Moreover, the downhill OER pathway at $U = 1.48$ V also indicates that the lower overpotential (merely 250 mV) arises due to the C2 active site on the surface.[33]

CONCLUSIONS

In summary, we have fabricated a novel thiadiazole-based covalent organic framework, C4-SHz COF, through the Schiff base condensation polymerization reaction between 1,3,5-tris(4-formylphenyl)benzene and 2,5-dihydrazinyl-1,3,4-thiadiazole under vacuum in a sealed tube. The resultant material displayed a unique molecular architecture, high porosity, BET surface area, and accessible active sites, which could enable this COF as a superior self-supported metal-free OER electrocatalyst. In the alkaline system, the material showed a low onset potential of 270 mV, and the material achieved a current density of 10 mA/cm^2 with a lower overpotential of 320 mV. The accomplished OER activity is comparable to other best reported metal-free catalysts with excellent durability. Therefore, the catalytic performance exhibited by C4-SHz COF suggests that it may replace metal-free carbon-based nanomaterials and could be a promising electrocatalyst for future energy conversion from abundant water resources.

ASSOCIATED CONTENT

Supporting Information

The Supporting Information is available free of charge at https://pubs.acs.org/doi/10.1021/acscatal.9b05470.

Materials, methods and characterization tools, experimental details, Pawley refined powder X-ray profile with other related data, simulated N_2 adsorption isotherm, TGA profile, comparison table with other reported catalysts, CV plot of materials before LSV measurement, *iR*-corrected LSV curve, exchange current density plot, RRDE measurement plot, ECSA plot, stability at different density plot, PXRD and FTIR of used COF materials, and computational OER mechanism related data (PDF)

(PDF)

AUTHOR INFORMATION

Corresponding Authors

Bikash Kumar Jena − *Material Chemistry Department, CSIR-Institute of Minerals and Materials Technology, Bhubaneswar 751013, India; Academy of Scientific & Innovative Research (AcSIR), Ghaziabad 201002, India;* orcid.org/0000-0003-1794-4430; Email: msab@iacs.res.in

Asim Bhaumik − *School of Materials Sciences, Indian Association for the Cultivation of Science, Jadavpur 700032, India;* orcid.org/0000-0002-4907-7418; Email: bikash@immt.res.in

Authors

Sujan Mondal − *School of Materials Sciences, Indian Association for the Cultivation of Science, Jadavpur 700032, India*

Bishnupad Mohanty − *Material Chemistry Department, CSIR-Institute of Minerals and Materials Technology, Bhubaneswar 751013, India;* orcid.org/0000-0001-7320-1223

Maryam Nurhuda − *School of Science and Technology, Nottingham Trent University, NG11 8NS Nottingham, U.K.*

Sasanka Dalapati − *Institute of Chemical Technology-Indian Oil Odisha Campus (ICT-IOC), Bhubaneswar, Odisha 751013, India*

Rajkumar Jana − *School of Physical Sciences, Indian Association for the Cultivation of Science, Jadavpur 700032, India*

https://dx.doi.org/10.1021/acscatal.9b05470
ACS Catal. XXXX, XXX, XXX−XXX

Matthew Addicoat − *School of Science and Technology, Nottingham Trent University, NG11 8NS Nottingham, U.K.;* orcid.org/0000-0002-5406-7927

Ayan Dutta − *School of Physical Sciences, Indian Association for the Cultivation of Science, Jadavpur 700032, India;* orcid.org/0000-0001-6723-087X

Complete contact information is available at: https://pubs.acs.org/10.1021/acscatal.9b05470

Author Contributions

[▽]S.M. and B.M. contributed equally. All authors have given approval to the final version of the manuscript.

Notes

The authors declare no competing financial interest.

■ ACKNOWLEDGMENTS

S.M. acknowledges CSIR, New Delhi, India. A.B. acknowledges DST-SERB, New Delhi, for a core research grant. Assistance from CSS, IACS Kolkata is acknowledged. M.A. acknowledges support from EPSRC, EP/S015868/1, and HPC resources on Thomas via the Materials Chemistry Consortium, EP/P020194. B.P.M. is grateful to UGC, New Delhi, for the fellowship, and B.K.J. is grateful to MNRE, New Delhi, BRNS, Mumbai, India, and CSIR, New Delhi, India, for the financial support.

■ REFERENCES

(1) Roger, I.; Shipman, M. A.; Symes, M. D. Earth-Abundant Catalysts for Electrochemical and Photoelectrochemical Water Splitting. *Nat. Rev. Chem.* **2017**, *1*, 1−13.

(2) Zhang, J.; Zhao, Z.; Xia, Z.; Dai, L. A Metal-Free Bifunctional Electrocatalyst for Oxygen Reduction and Oxygen Evolution Reactions. *Nat. Nanotechnol.* **2015**, *10*, 444−452.

(3) Liu, X.; Dai, L. Carbon-Based Metal-Free Catalysts. *Nat. Rev. Mater.* **2016**, *1*, 16064−16076.

(4) Mohanty, B.; Jena, B. K.; Basu, S. Single Atom on the 2D Matrix: An Emerging Electrocatalyst for Energy Applications. *ACS Omega* **2020**, *5*, 1287−1295.

(5) Kamila, S.; Mohanty, B.; Samantara, A. K.; Guha, P.; Ghosh, A.; Jena, B.; Satyam, P. V.; Mishra, B. K.; Jena, B. K. Highly Active 2D Layered MoS_2-rGO Hybrids for Energy Conversion and Storage Applications. *Sci. Rep.* **2017**, *7*, 8378−8313.

(6) Bhanja, P.; Mohanty, B.; Patra, A. K.; Ghosh, S.; Jena, B. K.; Bhaumik, A. IrO_2 and Pt Doped Mesoporous SnO_2 Nanospheres as Efficient Electrocatalysts for the Facile OER and HER. *ChemCatChem* **2019**, *11*, 583−592.

(7) Siracusano, S.; Van Dijk, N.; Payne-Johnson, E.; Baglio, V.; Aricò, A. S. Nanosized IrO_x and $IrRuO_x$ Electrocatalysts for the O_2 Evolution Reaction in PEM Water Electrolysers. *Appl. Catal. B: Environ.* **2015**, *164*, 488−495.

(8) Kayal, U.; Mohanty, B.; Bhanja, P.; Chatterjee, S.; Chandra, D.; Hara, M.; Kumar Jena, B.; Bhaumik, A. Ag Nanoparticle-Decorated, Ordered Mesoporous Silica as an Efficient Electrocatalyst for Alkaline Water Oxidation Reaction. *Dalton Trans.* **2019**, *48*, 2220−2227.

(9) Mohanty, B.; Ghorbani-Asl, M.; Kretschmer, S.; Ghosh, A.; Guha, P.; Panda, S. K.; Jena, B.; Krasheninnikov, A. V.; Jena, B. K. MoS_2 Quantum Dots as Efficient Catalyst Materials for the Oxygen Evolution Reaction. *ACS Catal.* **2018**, *8*, 1683−1689.

(10) Guo, H.-P.; Ruan, B.-Y.; Luo, W.-B.; Deng, J.; Wang, J.-Z.; Liu, H.-K.; Dou, S.-X. Ultrathin and Edge-Enriched Holey Nitride Nanosheets as Bifunctional Electrocatalysts for the Oxygen and Hydrogen Evolution Reactions. *ACS Catal.* **2018**, *8*, 9686−9696.

(11) Dutta, A.; Samantara, A. K.; Dutta, S. K.; Jena, B. K.; Pradhan, N. Surface-Oxidized Dico-balt Phosphide Nanoneedles as a Nonprecious, Durable, and Efficient OER Catalyst. *ACS Energy Lett.* **2016**, *1*, 169−174.

(12) Dalai, N.; Mohanty, B.; Mitra, A.; Jena, B. Highly Active Ternary Nickel-Iron Oxide as Bifunctional Catalyst for Electrochemical Water Splitting. *ChemistrySelect* **2019**, *4*, 7791−7796.

(13) Wu, H.; Yang, T.; Du, Y.; Shen, L.; Ho, G. W. Identification of Facet-Governing Reactivity in Hematite for Oxygen Evolution. *Adv. Mater.* **2018**, *30*, 1804341−1804349.

(14) Hu, Q.; Li, G.; Liu, X.; Zhu, B.; Chai, X.; Zhang, Q.; Liu, J.; He, C. Superhydrophilic Phytic-Acid-Doped Conductive Hydrogels as Metal-Free and Binder-Free Electrocatalysts for Efficient Water Oxidation. *Angew. Chem., Int. Ed.* **2019**, *58*, 4318−4322.

(15) Lai, J.; Li, S.; Wu, F.; Saqib, M.; Luque, R.; Xu, G. Unprecedented Metal-Free 3D Porous Carbonaceous Electrodes for Full Water Splitting. *Energy Environ. Sci.* **2016**, *9*, 1210−1214.

(16) Zhao, Y.; Yang, N.; Yao, H.; Liu, D.; Song, L.; Zhu, J.; Li, S.; Gu, L.; Lin, K.; Wang, D. Stereodefined Codoping of Sp-N and S Atoms in Few-Layer Graphdiyne for Oxygen Evolution Reaction. *J. Am. Chem. Soc.* **2019**, *141*, 7240−7244.

(17) Li, Q.; Yang, C.; Wu, L.; Wang, H.; Cui, X. Converting Benzene into γ-Graphyne and Its Enhanced Electrochemical Oxygen Evolution Performance. *J. Mater. Chem. A* **2019**, *7*, 5981−5990.

(18) Côté, A. P.; Benin, A. I.; Ockwig, N. W.; O'Keeffe, M.; Matzger, A. J.; Yaghi, O. M. Porous, crystalline, covalent organic frameworks. *Science* **2005**, *310*, 1166−1170.

(19) Song, Y.; Sun, Q.; Aguila, B.; Ma, S. Opportunities of Covalent Organic Frameworks for Advanced Applications. *Adv. Sci.* **2019**, *6*, 1801410.

(20) Ding, S. Y.; Wang, W. Covalent organic frameworks (COFs): from design to applications. *Chem. Soc. Rev.* **2013**, *42*, 548−568.

(21) Zhou, J.; Wang, B. Emerging Crystalline Porous Materials as a Multifunctional Platform for Electrochemical Energy Storage. *Chem. Soc. Rev.* **2017**, *46*, 6927−6945.

(22) Gomes, R.; Bhaumik, A. A New Triazine Functionalized Luminescent Covalent Organic Framework for Nitroaromatic Sensing and CO_2 Storage. *RSC Adv* **2016**, *6*, 28047−28054.

(23) Briega-Martos, V.; Ferre-Vilaplana, A.; de la Peña, A.; Segura, J. L.; Zamora, F.; Feliu, J. M.; Herrero, E. An Aza-Fused π-Conjugated Microporous Framework Catalyzes the Production of Hydrogen Peroxide. *ACS Catal.* **2017**, *7*, 1015−1024.

(24) Jin, E.; Asada, M.; Xu, Q.; Dalapati, S.; Addicoat, M. A.; Brady, M. A.; Xu, H.; Nakamura, T.; Heine, T.; Chen, Q.; Jiang, D. Two-dimensional sp^2carbon-conjugated covalent organic frameworks. *Science* **2017**, *357*, 673−676.

(25) Wang, H.; Zeng, Z.; Xu, P.; Li, L.; Zeng, G.; Xiao, R.; Tang, Z.; Huang, D.; Tang, L.; Lai, C.; et al. Recent Progress in Covalent Organic Framework Thin Films: Fabrications, Applications and Perspectives. *Chem. Soc. Rev.* **2019**, *48*, 488−516.

(26) Valentino, L.; Matsumoto, M.; Dichtel, W. R.; Mariñas, B. J. *Environ. Sci. Technol.* **2017**, *51*, 14352−14359.

(27) Lohse, M. S.; Bein, T. Covalent Organic Frameworks: Structures, Synthesis, and Applications. *Adv. Funct. Mater.* **2018**, *28*, 1705553.

(28) Mullangi, D.; Dhavale, V.; Shalini, S.; Nandi, S.; Collins, S.; Woo, T.; Kurungot, S.; Vaidhyanathan, R. Low-Overpotential Electrocatalytic Water Splitting with Noble-Metal-Free Nanoparticles Supported in a sp^3N-Rich Flexible COF. *Adv. Energy Mater.* **2016**, *6*, 1600110.

(29) Kamiya, K.; Kamai, R.; Hashimoto, K.; Nakanishi, S. Platinum-Modified Covalent Triazine Frameworks Hybridized with Carbon Nanoparticles as Methanol-Tolerant Oxygen Reduc-tion Electrocatalysts. *Nat. Commun.* **2014**, *5*, 5040.

(30) Aiyappa, H. B.; Thote, J.; Shinde, D. B.; Banerjee, R.; Kurungot, S. Cobalt-Modified Covalent Organic Framework as a Robust Water Oxidation Electrocatalyst. *Chem. Mater.* **2016**, *28*, 4375−4379.

(31) Wu, D.; Xu, Q.; Qian, J.; Li, X.; Sun, Y. Bimetallic Covalent Organic Frameworks for Constructing Multifunctional Electrocatalyst. *Chem. − Eur. J.* **2019**, *25*, 3105−3111.

(32) Sick, T.; Hufnagel, A. G.; Kampmann, J.; Kondofersky, I.; Calik, M.; Rotter, J. M.; Evans, A.; Döblinger, M.; Herbert, S.; Peters, K.; Böhm, D.; Knochel, P.; Medina, D. D.; Fattakhova-Rohlfing, D.; Bein,

T. Oriented Films of Conjugated 2D Covalent Organic Frameworks as Photocathodes for Water Splitting. *J. Am. Chem. Soc.* **2017**, *140*, 2085−2092.

(33) Yang, C.; Yang, Z.-D.; Dong, H.; Sun, N.; Lu, Y.; Zhang, F.-M.; Zhang, G. Theory-Driven Design and Targeting Synthesis of a Highly-Conjugated Basal-Plane 2D Covalent Organic Framework for Metal-Free Electrocatalytic OER. *ACS Energy Lett.* **2019**, *4*, 2251−2258.

(34) Sick, T.; Rotter, J. M.; Reuter, S.; Kandambeth, S.; Bach, N. N.; Döblinger, M.; Merz, J.; Clark, T.; Marder, T. B.; Bein, T.; Medina, D. D. Switching on and off Interlayer Correlations and Porosity in 2D Covalent Organic Frameworks. *J. Am. Chem. Soc.* **2019**, *141*, 12570−12581.

(35) Mondal, S.; Kundu, S. K.; Bhaumik, A. A Facile Approach for the Synthesis of Hydroxyl-Rich Microporous Organic Networks for Efficient CO_2 Capture and H_2 Storage. *Chem. Commun.* **2017**, *53*, 2752−2755.

(36) Bandyopadhyay, S.; Anil, A. G.; James, A.; Patra, A. Multifunctional Porous Organic Polymers: Tuning of Porosity, CO_2, and H_2 Storage and Visible-Light-Driven Photocatalysis. *ACS Appl. Mater. Interfaces* **2016**, *8*, 27669−27678.

(37) Ji, G.; Yang, Z.; Zhang, H.; Zhao, Y.; Yu, B.; Ma, Z.; Liu, Z. Hierarchically Mesoporous O-Hydroxyazobenzene Polymers: Synthesis and Their Applications in CO_2 Capture and Conversion. *Angew. Chem., Int. Ed.* **2016**, *55*, 9685−9689.

(38) Liu, F.; Huang, K.; Yoo, C.-J.; Okonkwo, C.; Tao, D.-J.; Jones, C. W.; Dai, S. Facilely Synthesized Meso-Macroporous Polymer as Support of Poly (Ethyleneimine) for Highly Efficient and Selective Capture of CO_2. *Chem. Eng. J.* **2017**, *314*, 466−476.

(39) Dalapati, S.; Addicoat, M.; Jin, S.; Sakurai, T.; Gao, J.; Xu, H.; Irle, S.; Seki, S.; Jiang, D. Rational Design of Crystalline Supermicroporous Covalent Organic Frameworks with Triangular Topologies. *Nat. Commun.* **2015**, *6*, 7786.

(40) Merí-Bofí, L.; Royuela, S.; Zamora, F.; Ruiz-González, M. L.; Segura, J. L.; Muñoz-Olivas, R.; Mancheño, M. J. Thiol grafted imine-based covalent organic frameworks for water re-mediation through selective removal of Hg(II). *J. Mater. Chem. A* **2017**, *5*, 17973−17981.

(41) Gao, Q.; Li, X.; Ning, G.-H.; Leng, K.; Tian, B.; Liu, C.; Tang, W.; Xu, H.-S.; Loh, K. P. Highly photoluminescent two-dimensional imine-based covalent organic frameworks for chemical sensing. *Chem. Commun.* **2018**, *54*, 2349−2352.

(42) Waller, P. J.; Gándara, F.; Yaghi, O. M. Chemistry of Covalent Organic Frameworks. *Acc. Chem. Res.* **2015**, *48*, 3053−3063.

(43) Mondal, S.; Chatterjee, S.; Mondal, S.; Bhaumik, A. Thioether-Functionalized Covalent Triazine Nanospheres: A Robust Adsorbent for Mercury Removal. *ACS Sustainable Chem. Eng.* **2019**, *7*, 7353−7361.

(44) Mohanty, B.; Wei, Y.; Ghorbani-Asl, M.; Krasheninnikov, A. V.; Rajput, P.; Jena, B. K. Revealing the Defect-dominated Oxygen Evolution Activity of Hematene. *J. Mater. Chem. A* **2020**, *8*, 6709.

(45) Zhao, S.; Wang, Y.; Dong, J.; He, C.-T.; Yin, H.; An, P.; Zhao, K.; Zhang, X.; Gao, C.; Zhang, L.; Lv, J.; Wang, J.; Zhang, J.; Khattak, A. M.; Khan, N. A.; Wei, Z.; Zhang, J.; Liu, S.; Zhao, H.; Tang, Z. Ultrathin Metal-organic Framework nanosheets for Electrocatalytic Oxygen Evolution. *Nat. Energy* **2016**, *1*, 16184.

(46) Wu, X.; Yang, Y.; Zhang, T.; Wang, B.; Xu, H.; Yan, X.; Tang, Y. *ACS Appl. Mater. Interfaces* **2019**, *11*, 39841−39847.

(47) Bothra, P.; Pati, S. K. Activity of Water Oxidation on Pure and (Fe, Ni, and Cu)-Substituted Co_3O_4. *ACS Energy Lett.* **2016**, *1*, 858−862.

(48) Wang, Q.; Ji, Y.; Lei, Y.; Wang, Y.; Wang, Y.; Li, Y.; Wang, S. Pyridinic-N-Dominated Doped Defective Graphene as a Superior Oxygen Electrocatalyst for Ultrahigh-Energy-Density Zn-Air Batteries. *ACS Energy Lett.* **2018**, *3*, 1183−1191.

(49) Yang, H. B.; Miao, J.; Hung, S.-F.; Chen, J.; Tao, H. B.; Wang, X.; Zhang, L.; Chen, R.; Gao, J.; Chen, H. M.; Dai, L.; Liu, B. Identification of Catalytic Sites for Oxygen Reduction and Oxygen Evolution in N-doped Graphene Materials: Development of Highly Efficient Metal-free Bifunctional Electrocatalyst. *Sci. Adv.* **2016**, *2*, e1501122−e1501132.

https://dx.doi.org/10.1021/acscatal.9b05470
ACS Catal. XXXX, XXX, XXX−XXX